

Design and simulations of a resonant accelerometer

Yan Li¹ · Guo Zhan-She² · Yuanyuan Qu¹ · Yunjiu Zhang¹

Received: 27 May 2017 / Accepted: 17 August 2017 / Published online: 4 September 2017
© Springer-Verlag GmbH Germany 2017

Abstract A resonant accelerometer was designed and simulated in detail. The structure was composed of external frame and internal structure. The internal structure consists of a single proof mass, a pair of resonators and elastic beams. Structure design is implemented by taking advantage of the finite element analyses. From the simulation results we can see that the design of external frame, should ensure that the frame in line with the “beam” characteristics, and increase its stiffness under this condition. The design of internal structure, should ensure that the resonant beam stiffness, sensitivity, vertical vibration and range. Moreover, simulation results reveal the resonant accelerometer linearity is better under the condition of $|F| < 5$ N, the range is ± 25 g and the sensitivity is 272.5 Hz/g. All these simulations above can verify the high performance accelerometer by simple and optimized structure design.

1 Introduction

Resonant accelerometer, their operational principle is detecting resonant frequency shift in the resonator. Detection of frequency shift is more advantageous compared to detecting changes in amplitude, as it less sensitive to effects such as feedthrough coupling from undesired sources and parasitic passive elements (Zou and Seshia 2015; Pedersen

and Seshia 2004; Seshia et al. 2002). Thus, as one core device of an inertial navigation system, its precision and quality of property greatly determine the precision and property of the inertial navigation system. The system is widely applied to missile, satellites, rockets, and other aircraft and plays a significant part in guaranteeing the vehicle attitude being stable and the target being accurate (Comi et al. 2010; Suminto 1996). Recently, there are several reports on accelerometer of the novel structures (Wang et al. 2017; Zhao et al. 2016; Ding et al. 2016a, b; Zhang et al. 2015; Yang et al. 2014; Park et al. 2014), measurement methods (Li et al. 2017; Comi et al. 2016; Yan et al. 2016; Park et al. 2016; Zotov et al. 2015; Heng and Li 2013; Shi et al. 2013) and fabricating process (Verma et al. 2016; Han et al. 2013). By the investigation and analysis about the existing literature dates and relevant technologies, it can be found that there are very few studies about external frame and internal structure to design the resonant accelerometer structure.

This paper focuses on the design and simulation of a resonant accelerometer. The structure of the resonant accelerometer is designed according to the external frame and internal structure. The acceleration on proof mass determines the resonance frequency shifts of a pair of resonator, which are proportional to the external acceleration. The pairs of decoupling resonators allow the simultaneous differential measurement of acceleration along two orthogonal axes, while the high sensitivity and low cross-axis sensitivity is guaranteed.

2 Operational principle

The working principle of the resonant accelerometer is shown in Fig. 1, which mainly consists of a single proof mass, a pair of resonators, levers and elastic beams. When

✉ Guo Zhan-She
guozhanshe@buaa.edu.cn

¹ School of Mechanical Electronic and Information Engineering, China University of Mining and Technology, Beijing 100083, China

² School of Instrument Science and Opto-electronics Engineering, Beihang University, Beijing 100191, China

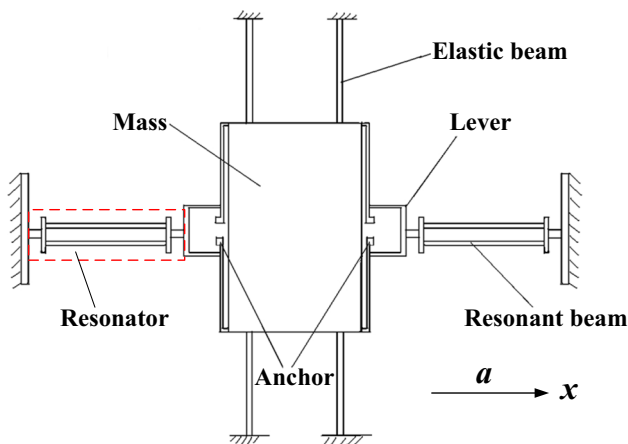


Fig. 1 The working principle of the resonant accelerometer

acceleration a is produced in the x direction, in the light of Newton’s second law, this direction will produce an inertia force that can be represented as:

$$F = ma. \tag{1}$$

In this case, m is mass of the proof mass, F is the inertial force. The acceleration is converted to the inertial forces along the x axis, and the inertia force is applied to the axis of the resonator, changing the original resonant frequency of the resonant beam. According to the theoretical derivation, the corresponding acceleration is obtained by measuring the variation of vibration resonant frequency of the new resonant state.

When the resonant beam vibrate, the natural resonant frequency is:

$$\omega_n = \sqrt{k_{\text{eff}}/M_{\text{eff}}}, \tag{2}$$

where k_{eff} is the equivalent stiffness of the resonator and M_{eff} is the equivalent mass of the resonant beam.

Assume that the natural resonant frequency of the resonant beam can be expressed as:

$$\omega'_n = \omega_n \sqrt{1 + \beta a}. \tag{3}$$

In this case, β is a constant relative to the accelerometer structure. To show the Eq. (3) in the form of Taylor series:

$$\omega'_n = \omega_n \left(1 + \frac{1}{2} \beta a - \frac{1}{8} \beta^2 a^2 + \frac{1}{16} \beta^3 a^3 - \dots \right). \tag{4}$$

Therefore, in the case of higher order terms, the frequency variation of the resonator under the measured acceleration a is:

$$\Delta\omega = \omega'_n - \omega_n = \frac{1}{2} \beta a \omega_n. \tag{5}$$

It can be seen from the Eq. (5), in a certain acceleration input range, the measured acceleration is linearly proportional to the change in natural resonant frequency.

Therefore, the measurement of the measured acceleration can be achieved by measuring the variation in the natural resonant frequency. However, the high order terms of the acceleration a in the Eq. (4) influences the linearity of the accelerometer scale factor. That is, the linear degree of the accelerometer is determined by the nonlinearity of the change in frequency in terms of $1/8\beta^2 a^2$ and its subsequent terms. The influence of higher order terms on $\Delta\omega$ are negligible by properly designing the value of β .

3 Structure design and simulations

In order to realize the measurement of high performance accelerometer by simple and optimized structure design, this paper divides the resonant accelerometer structure into two parts, namely the external frame and the internal structure, as shown in Fig. 2, in which the internal structure includes the mass, resonators and elastic beams.

The external frame mainly plays the role of supporting the internal structure, how to avoid the energy of the resonator transferred to the external frame, avoid the external frame’s vibration in the system operating frequency range, are problems that needs to be solved in the external frame design. The internal structure is the main body of the accelerometer, the sensitivity of the entire accelerometer is replaced by the sensitivity of the resonator in design. So in the actual design, establishing the whole structure of mechanical model and mathematical model, getting the relationship between force and frequency characteristics, and obtaining sensitivity formula by analysis of the structure.

3.1 External frame

The core idea of external frame design is that external structural rigidity is much greater than the internal structure, which can be decoupled from the internal structures. Figure 3 shows the structure of external frame, Fig. 4 shows the width of external frame beam. Take the

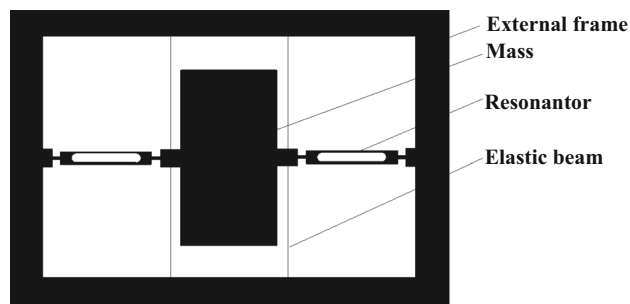


Fig. 2 The resonant accelerometer structure

microelements b_1, b_2 , on the side of the external frame. When b_1 increases, the equivalent of the microelement of the stiffness k_1 increases, reflected in the characteristics “board” of the external frame. When b_2 increases, the equivalent of the microelement of the stiffness k_2 is reduced, reflected in the characteristics “beam” of the external frame. And b_1, b_2 belong to the width of the beam, so, with b_1, b_2 increases, k_1, k_2 must have an intersection, and this point is the theoretical optimum width of the beam. The optimal design of external frame parameters was carried out with six sets of structural parameters. Table 1 shows the six sets of structural parameters, Figs. 5, 6, 7, 8, 9 and 10 show the modal simulations of the six structures, we can choose the optimization parameters of the external frame by comparing them.

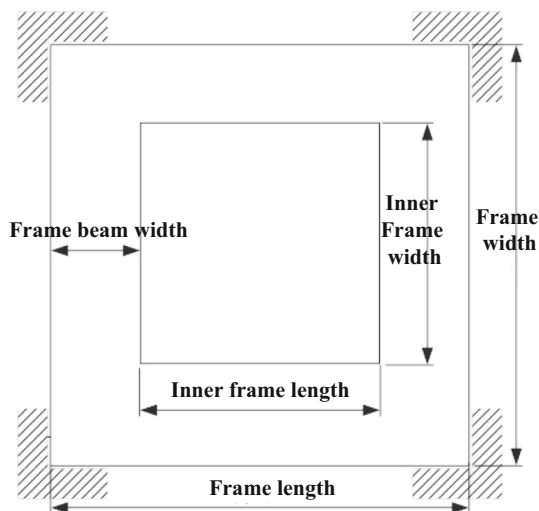


Fig. 3 The structure of the external frame

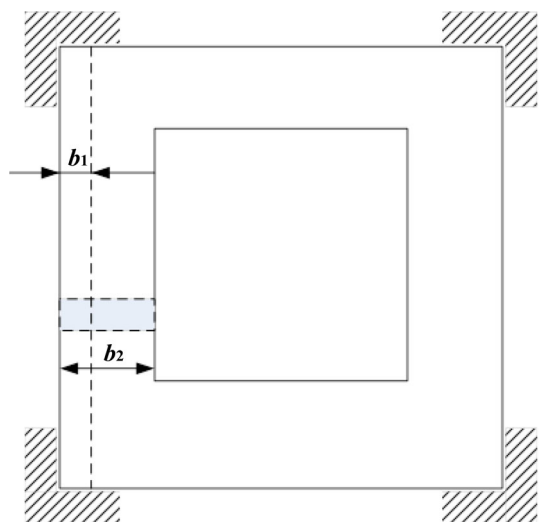


Fig. 4 The width of external frame beam

According to the simulation results, structures 3, 4 and 5 are the overall structure of the work with the frame beam width was 10 mm and the resonant beam width were 0.1, 0.2 and 0.3 mm. When the resonant beam width is gradually increased to 2 mm, its stiffness will increase gradually. At this time, the external frame and its stiffness ratio become smaller, resulting in the structure of the first ten modes did not appear working mode but the vibration of the external frame.

Structure 1, 2, 4, 6 are the overall structure of the work with the resonant beam size unchanged and the width of the frame beam were 1, 10 and 20 mm. Because the stiffness is smaller when the width of the external frame are 1 and 2.5 mm, the simulated figures show that the overall structure of the first order mode appears bending mode on each side of the frame, and the bending modes was similar to the beam bending mode, especially when the frame beam width was 1 mm, first ten order modes are not present work mode, at this time the system energy mainly concentrated in the vibration of the external frame. When the width of the frame becomes 20 mm, the first order mode of the whole structure shows that the frame is vibrating with the characteristics of the “board”. It can be seen, although the stiffness of the frame at this time increased, but the frame reflects the “board” characteristics. Therefore, the design of external frame, should ensure that the frame in line with the “beam” characteristics, and increase its stiffness under this condition.

3.2 Internal structure

Normally, the vertical vibration frequency of the system is much higher than the axial vibration frequency, so the effect of the system axial displacement is ignored when the system is modeled. When the internal structure of the resonant accelerometer is displaced in the axial direction of the resonator, the energy dissipates away from the inside of the resonator. Therefore, the appearance of the system vertical vibration should be avoided during the internal structure optimization.

Figure 11 shows the equivalent diagram of the internal structure, Figs. 12, 13, 14, 15, 16 and 17 show the simulations of the vertical vibration frequency from different internal structure parameters, and Table 2 shows the comparison between structural parameters and simulation results. From the results of structure 1–structure 3, it can be seen that the size of the equivalent resonant beam is constant. On the one hand, with the increase of the quality of the proof mass, the coupling from vertical vibration frequency to axial vibration frequency is enhanced, and the proof mass is displaced along the axial direction of the resonator. On the one hand, the increase in proof mass will boost the

Table 1 Structural parameters of the external frame

Structure	1	2	3	4	5	6	Unit
Density	7.8E3	7.8E3	7.8E3	7.8E3	7.8E3	7.8E3	kg/m ³
Young's modulus	2E11	2E11	2E11	2E11	2E11	2E11	Pa
External frame (length × width × thickness)	62 × 62 × 5	65 × 65 × 5	80 × 80 × 5	80 × 80 × 5	80 × 80 × 5	100 × 100 × 5	mm
Inner frame (length × width × thickness)	60 × 60 × 5	60 × 60 × 5	60 × 60 × 5	60 × 60 × 5	60 × 60 × 5	60 × 60 × 5	mm
Poisson ratio	0.3	0.3	0.3	0.3	0.3	0.3	/
Resonant beam (length × width × thickness)	20 × 0.2 × 5	20 × 0.2 × 5	20 × 0.1 × 5	20 × 0.2 × 5	20 × 2 × 5	20 × 0.2 × 5	mm
Proof mass (length × width × thickness)	20 × 10 × 5	20 × 10 × 5	20 × 10 × 5	20 × 10 × 5	20 × 10 × 5	20 × 10 × 5	mm

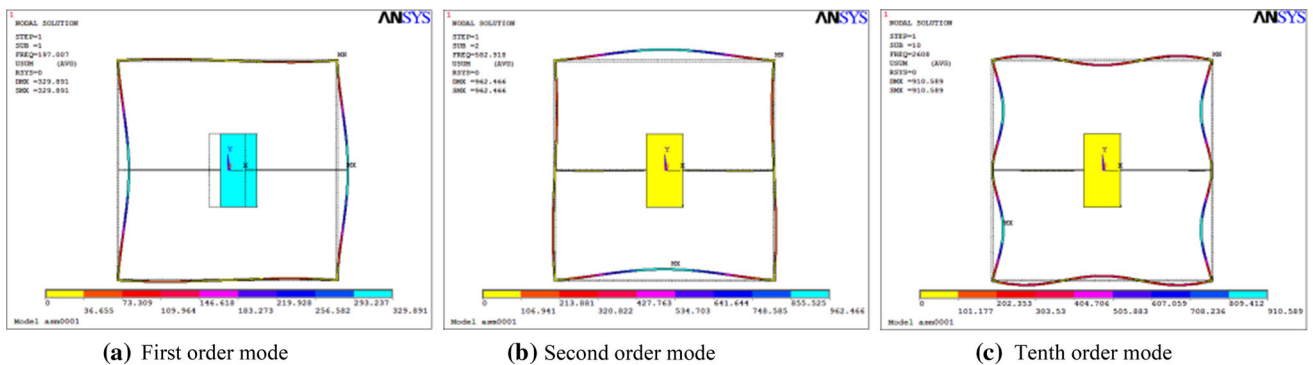


Fig. 5 Structure 1 modes

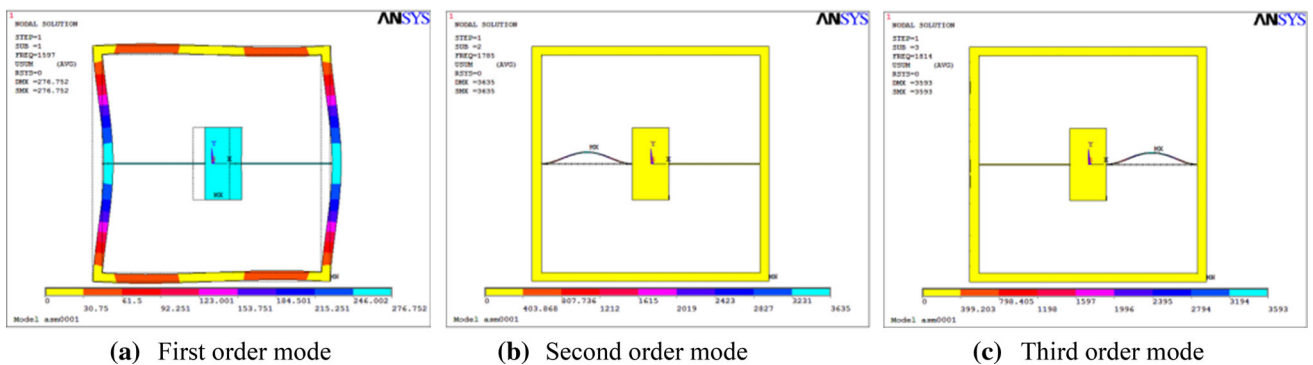


Fig. 6 Structure 2 modes

sensitivity of the system. Thus, the selection of proof mass must weigh the relationship between the resonant beam thickness and proof mass. From the simulated results of structure 4–structure 6, it can be seen that the coupling of the vertical vibration frequency to the axial vibration frequency increases with the decrease of the equivalent resonant beam thickness, that is, the decrease of the stiffness of the beam leads to the displacement of

the mass along the axial direction of the resonator, which dissipates energy outwards. Therefore, we should try to ensure that the equivalent resonant beam stiffness is relatively large. The sensitivity formula shows that the smaller the thickness of the resonant beam, the higher of the sensitivity, but too small beam thickness will lead to the emergence of vertical vibration, and narrow the accelerometer range.

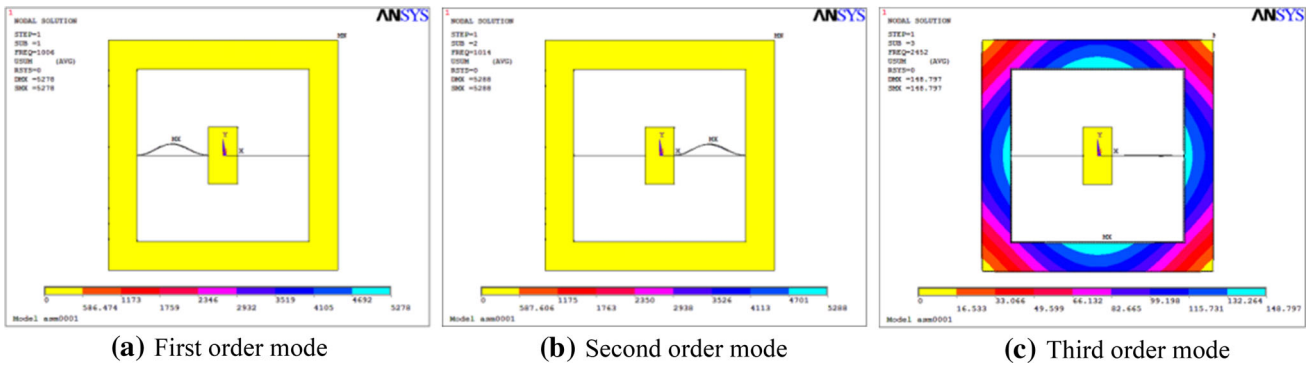


Fig. 7 Structure 3 modes

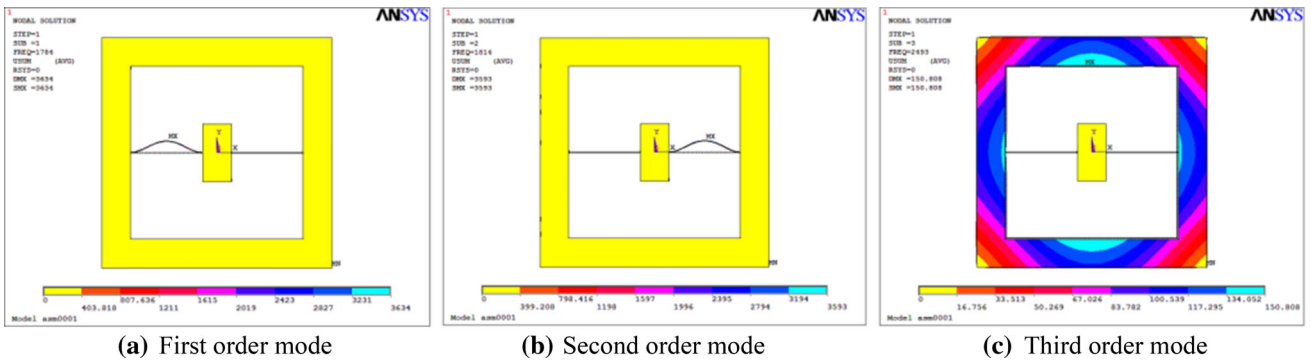


Fig. 8 Structure 4 modes

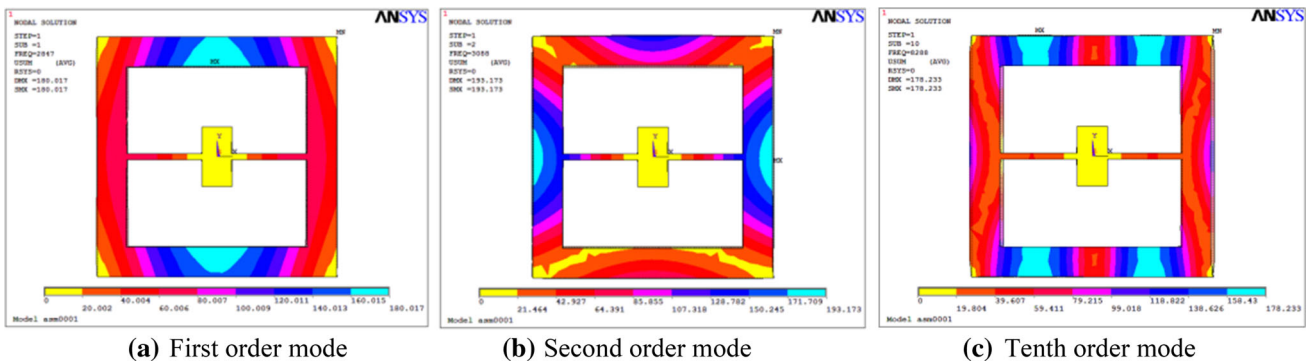


Fig. 9 Structure 5 modes

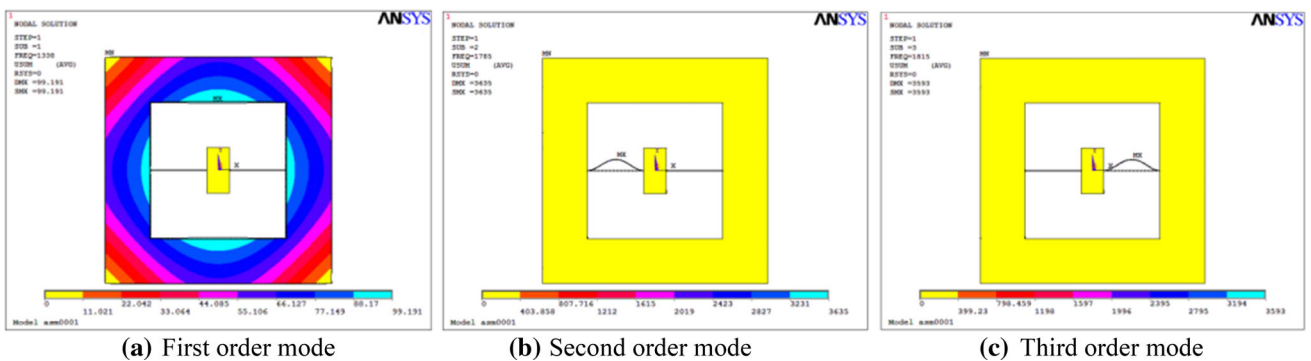


Fig. 10 Structure 6 modes

Fig. 11 Equivalent diagram of the internal structure

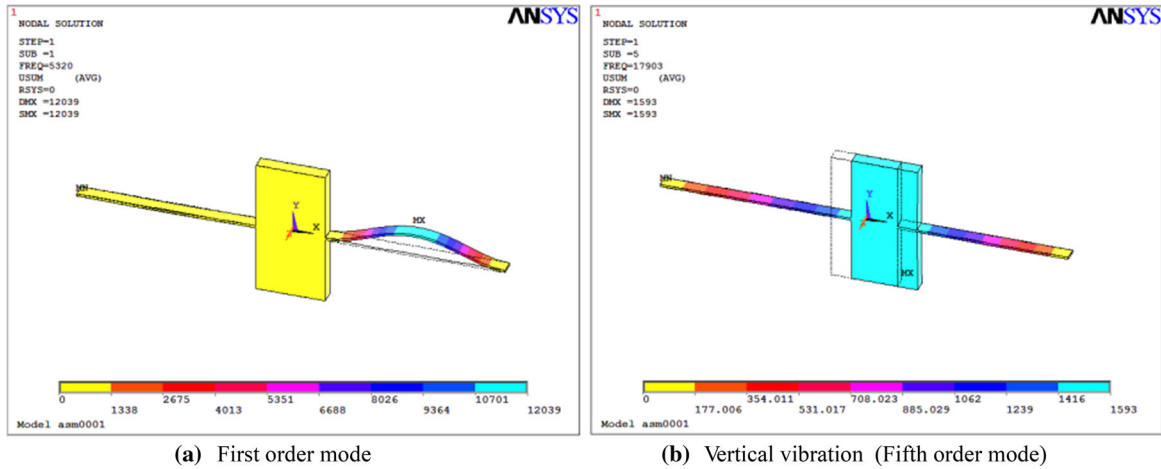
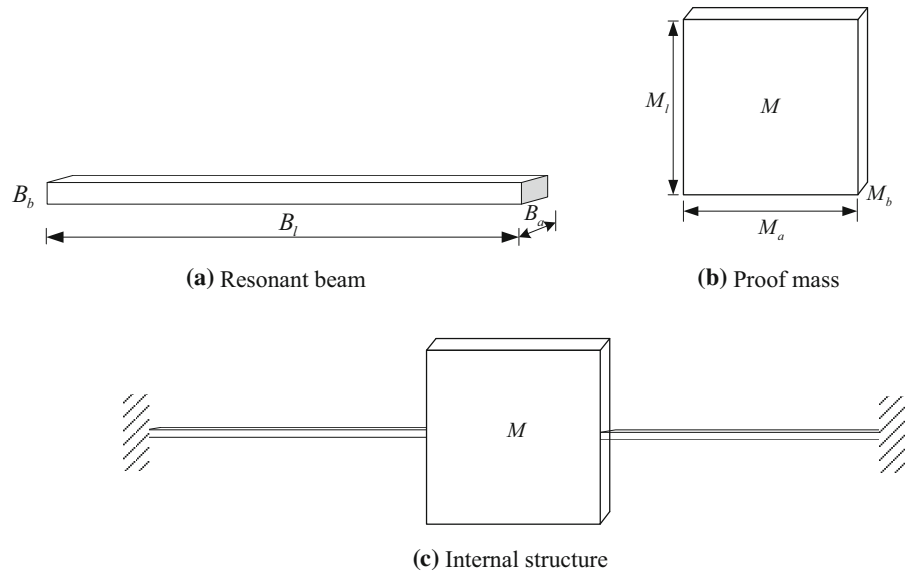


Fig. 12 Structure 1 modes

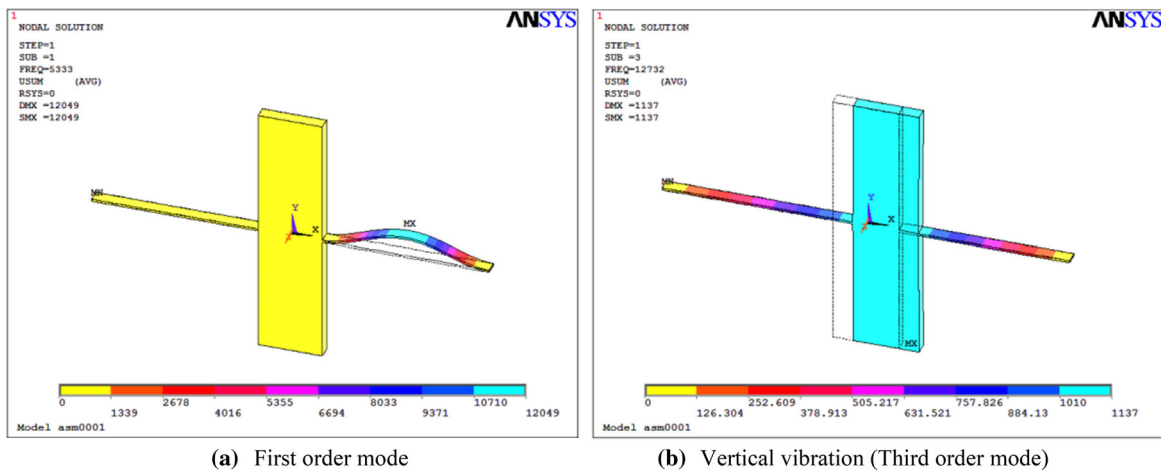


Fig. 13 Structure 2 modes

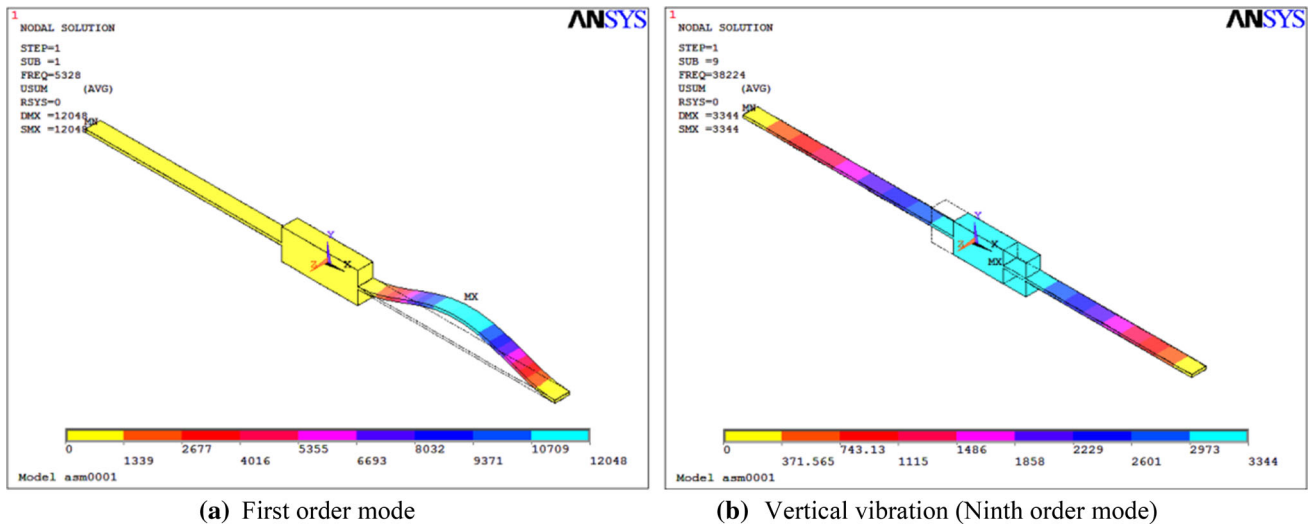


Fig. 14 Structure 3 modes

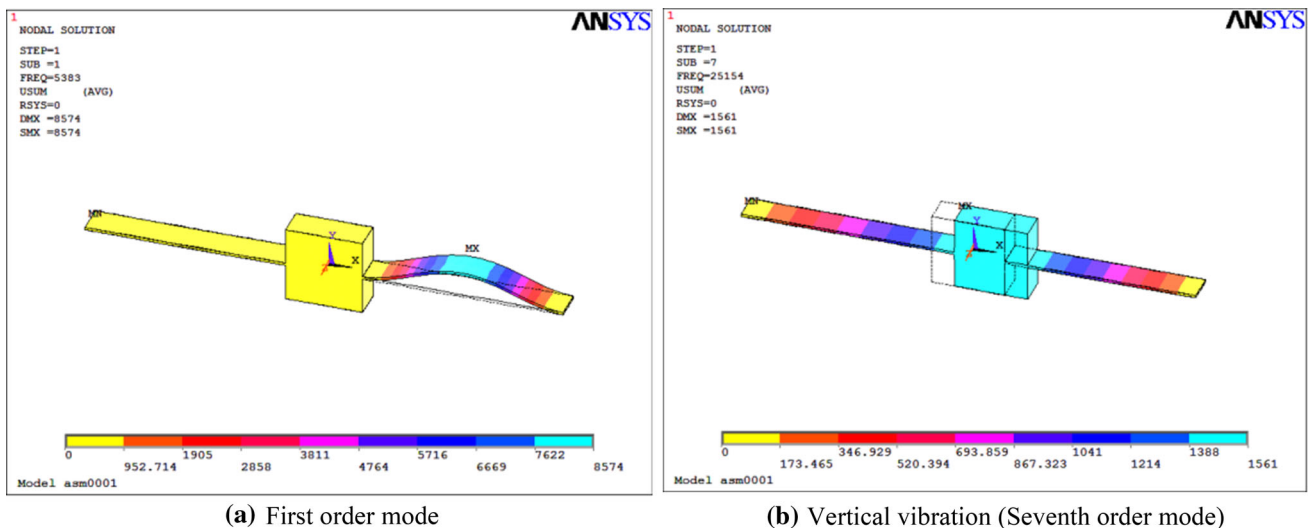


Fig. 15 Structure 4 modes

4 Performance simulations

From the above analysis, Table 3 shows the given internal structure parameters. From the analysis of the relationship between accelerometer and frequency, the equation of tension–frequency and pressure–frequency can be obtained, and the sensitivity curve of the whole structure can be obtained. As shown in Fig. 18, the blue line represents the tension–frequency curve and the red line represents the pressure–frequency curve.

In the tension–frequency and pressure–frequency equations, if $F = \eta \frac{EJ}{l^2}$, $P = \zeta \frac{\pi^2 \sqrt{\frac{EJ}{\rho A}}}{l^2}$, then the tension–frequency and pressure–frequency equations can be written as:

$$\begin{aligned}
 H_1 = & -\frac{1}{2} \sqrt{-2\eta + 2\sqrt{\eta^2 + 4\zeta^2 \pi^4}} \sqrt{2\eta + 2\sqrt{\eta^2 + 4\zeta^2 \pi^4}} \\
 & - \sin\left(\frac{1}{2} \sqrt{-2\eta + 2\sqrt{\eta^2 + 4\zeta^2 \pi^4}}\right) \\
 & \times \sinh\left(\frac{1}{2} \sqrt{-2\eta + 2\sqrt{\eta^2 + 4\zeta^2 \pi^4}}\right) \eta \\
 & + \frac{1}{2} \sqrt{-2\eta + 2\sqrt{\eta^2 + 4\zeta^2 \pi^4}} \sqrt{2\eta + 2\sqrt{\eta^2 + 4\zeta^2 \pi^4}} \\
 & \cdot \cos\left(\frac{1}{2} \sqrt{-2\eta + 2\sqrt{\eta^2 + 4\zeta^2 \pi^4}}\right) \\
 & \cdot \cosh\left(\frac{1}{2} \sqrt{2\eta + 2\sqrt{\eta^2 + 4\zeta^2 \pi^4}}\right) = 0,
 \end{aligned}$$

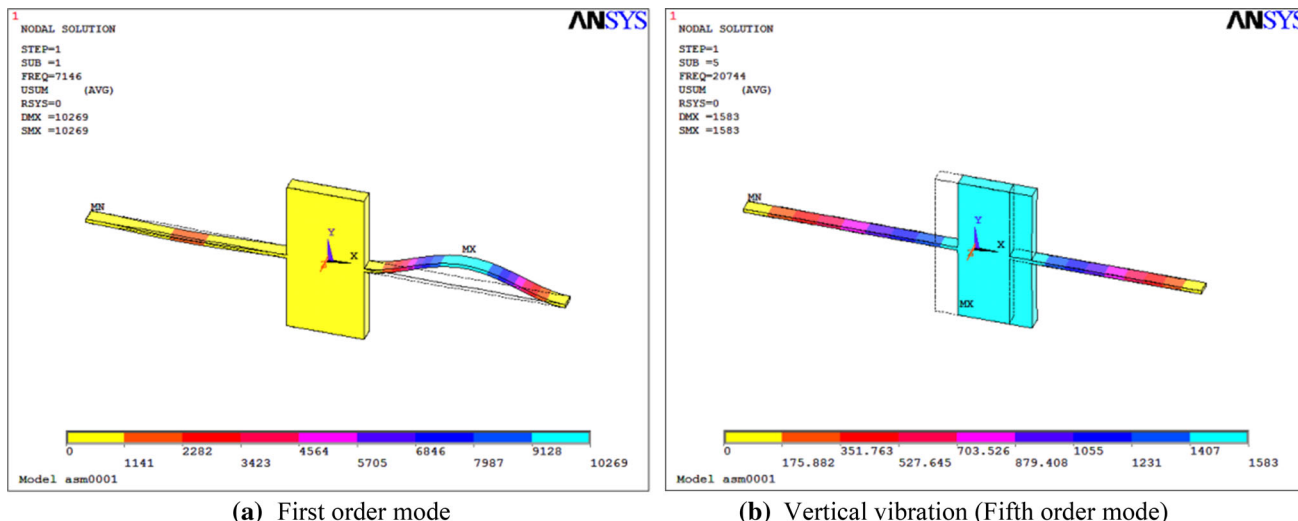


Fig. 16 Structure 5 modes

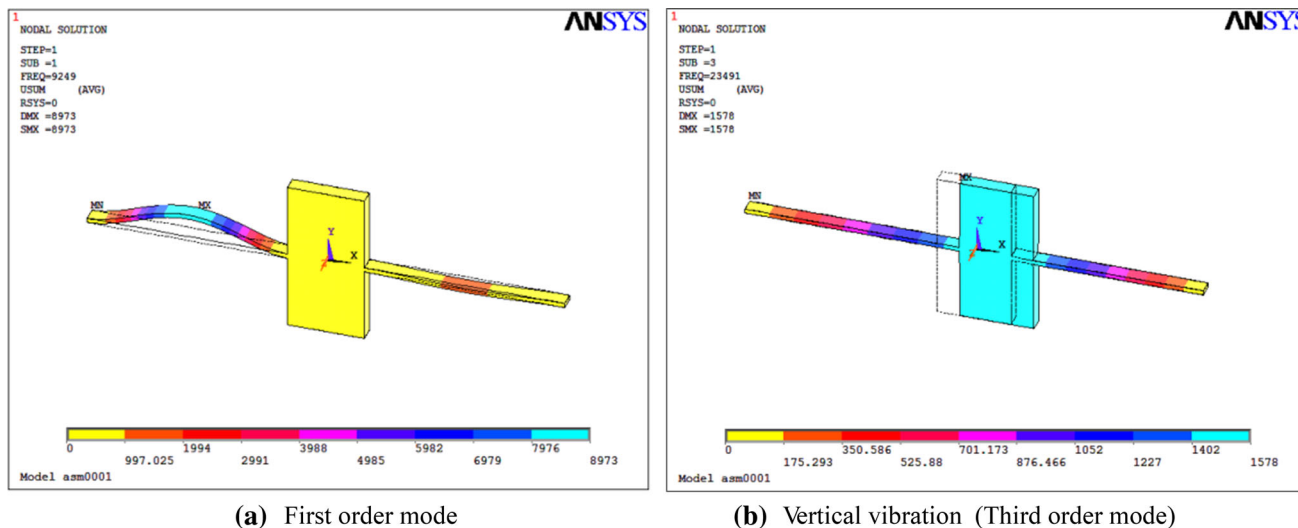


Fig. 17 Structure 6 modes

$$\begin{aligned}
 H_y = & -\frac{1}{2} \sqrt{-2\eta + 2\sqrt{\eta^2 + 4\zeta^2\pi^4}} \sqrt{2\eta + 2\sqrt{\eta^2 + 4\zeta^2\pi^4}} \\
 & - \sin\left(\frac{1}{2} \sqrt{2\eta + 2\sqrt{\eta^2 + 4\zeta^2\pi^4}}\right) \\
 & \times \sinh\left(\frac{1}{2} \sqrt{-2\eta + 2\sqrt{\eta^2 + 4\zeta^2\pi^4}}\right) \eta \\
 & + \frac{1}{2} \sqrt{2\eta + 2\sqrt{\eta^2 + 4\zeta^2\pi^4}} \sqrt{-2\eta + 2\sqrt{\eta^2 + 4\zeta^2\pi^4}} \\
 & \cdot \cos\left(\frac{1}{2} \sqrt{2\eta + 2\sqrt{\eta^2 + 4\zeta^2\pi^4}}\right) \\
 & \cdot \cosh\left(\frac{1}{2} \sqrt{-2\eta + 2\sqrt{\eta^2 + 4\zeta^2\pi^4}}\right) = 0.
 \end{aligned}$$

where E is the elastic modulus, J is the moment of inertia, l is the length of the beam, and A is the cross-sectional area of the beam, and η, ζ is arbitrary constants.

From $F_1(\eta, \zeta) = 0$, at $\eta = 0$, find the approximate solution of $\zeta = \zeta(\eta)$, that is, where the Taylor expansion is:

$$\begin{aligned}
 F_1(\eta, \zeta) = & 2.266887764 + 0.02785723822\eta \\
 & - 0.0003764\eta^2 + 0.00001441\eta^3.
 \end{aligned} \tag{6}$$

From $F_y(\eta, \zeta) = 0$, at $\eta = 0$, find the approximate solution of $\zeta = \zeta(\eta)$, that is, where the Taylor expansion is:

$$\begin{aligned}
 F_y(\eta, \zeta) = & 2.266887764 + 0.02785723822\eta \\
 & - 0.0003764\eta^2 + 0.00001441\eta^3.
 \end{aligned} \tag{7}$$

Therefore,

$$F_1(\eta, \zeta) - F_y(\eta, \zeta) = 0.0557\eta + 0.0002882\eta^3. \tag{8}$$

Table 2 The comparison between structural parameters and simulation results

	B_l	B_a	B_b	M_l	M_a	M_b	Vertical vibration frequency (order)	Working frequency
Structure1	13	1	0.17	10	5	1	17,903 (5)	5320
Structure2	13	1	0.17	20	5	1	12,732 (3)	5332
Structure3	13	1	0.17	2	5	1	38,224 (9)	5328
Structure4	13	1	0.05	10	5	1	9920 (7)	1598
Structure5	13	1	0.23	10	5	1	20,744 (5)	7146
Structure6	13	1	0.3	10	5	1	23,491 (3)	9249

Table 3 Internal structure parameters

Parameters	Value	Unit
Density	7.8E3	kg/m ³
Young’s modulus	2E11	Pa
Internal frame	100 × 100 × 5	mm ³
Poisson ratio	0.3	/
Resonant beam (length × width × thickness)	13 × 1 × 0.17	mm ³
Proof mass (length × width × thickness)	30 × 60 × 5	mm ³
Axial force	5	N

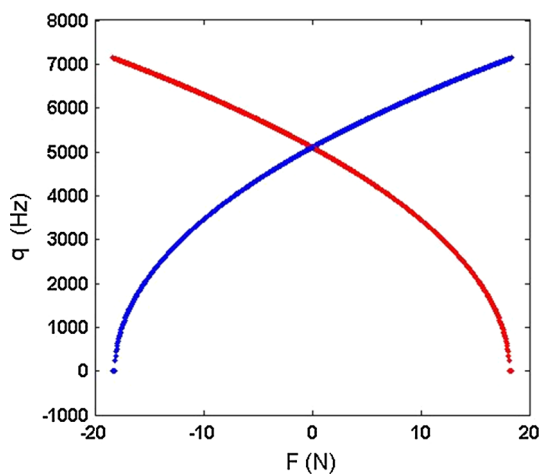


Fig. 18 Tension–frequency and pressure–frequency curves

Figure 19 shows the $\zeta - \eta$ relationship curve. From $\Delta\zeta = \Delta\zeta(\eta)$, we can see $\Delta p = \Delta p(F)$, therefore, the sensitivity curve of the overall structure is shown in Fig. 20. Where the solid line is the fitting curve, and its slope represents the sensitivity of the system. To further obtain the linear range of the resonant accelerometer, make the difference between the solid line and the dotted line in Figs. 20, and 21 is obtained. From Fig. 21, if $|F| < 5$ N, the system linearity is better, suitable for sensor measurement. Thus, the design of the resonant accelerometer range ± 25 g and the sensitivity of 272.5 Hz/g can be introduced according to the quality of the proof mass.

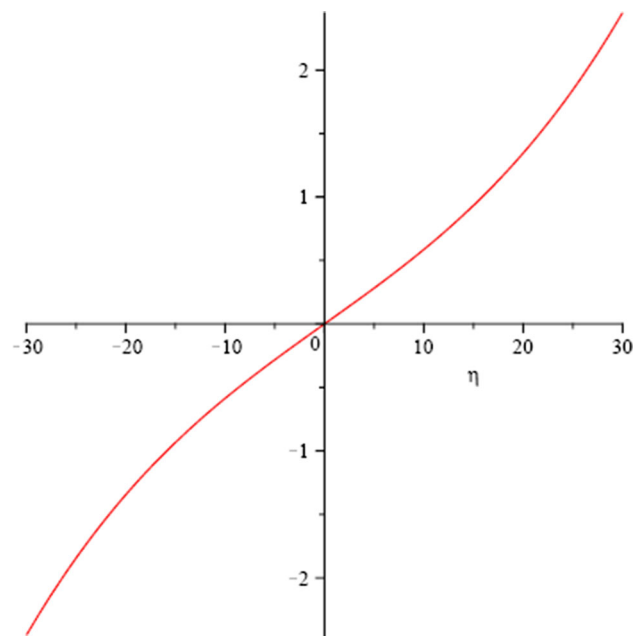


Fig. 19 The $\zeta - \eta$ relationship curve

5 Conclusions

A resonant accelerometer is designed and analyzed. The device is mainly composed of the external frame and internal structure. The external frame mainly plays the role of supporting the internal structure, internal structure is mainly composed of a single proof mass and two resonators, which provides acceleration measurement using

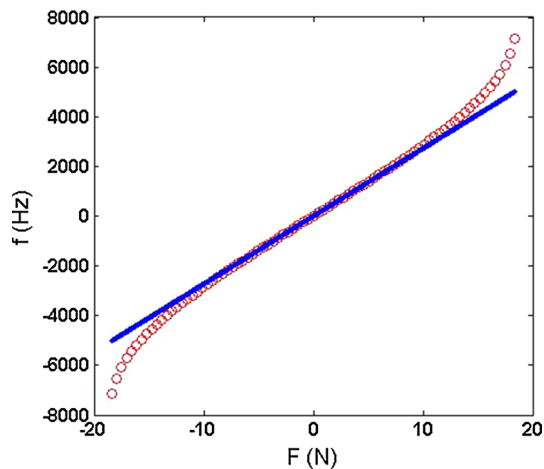


Fig. 20 The sensitivity curve of overall structure

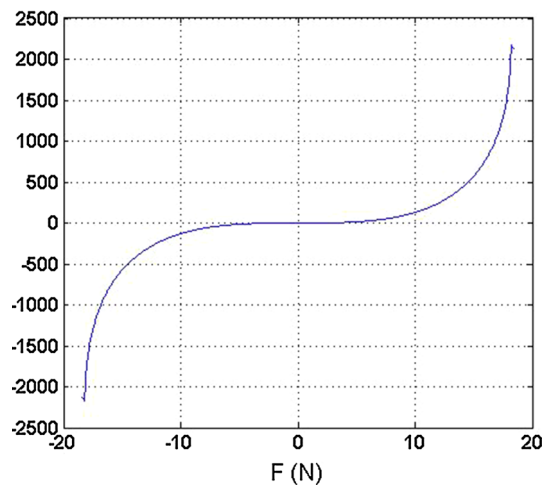


Fig. 21 The linear range of the resonant accelerometer

the decoupling resonators separately. The FEM simulations are performed by ANSYS software to verify the feasibility of the resonant accelerometer design. According to the simulation results, the design of external frame, should ensure that the frame in line with the “beam” characteristics and increase its stiffness. The design of internal structure, should ensure that the resonant beam stiffness, sensitivity, vertical vibration and range. The designed resonant accelerometer, if $|F| < 5$ N, the system linearity is better, suitable for sensor measurement, the range is ± 25 g and the sensitivity is 272.5 Hz/g. Although, the above conditions are predicted for the resonant accelerometer, the predictions can be easily translated to other resonant sensors designs.

Acknowledgements This study is supported by the National Natural Science Foundation of China under Grant no. 61503018.

References

- Comi C, Corigliano A, Langfelder G (2010) A resonant microaccelerometer with high sensitivity operating in an oscillating circuit. *J Microelectromech Syst* 19(5):1140–1152
- Comi C, Corigliano A, Langfelder G (2016) Sensitivity and temperature behavior of a novel z-axis differential resonant micro accelerometer. *J Micromech Microeng* 26(3):035006
- Ding H, Zhao J, Ju B-F (2016a) A high-sensitivity biaxial resonant accelerometer with two-stage microleverage mechanisms. *J Micromech Microeng* 26(1):015011
- Ding H, Zhao J, Ju B-F (2016b) A new analytical model of single-stage microleverage mechanism in resonant accelerometer. *Microsyst Technol Micro Nanosyst Inf Storage Process Syst* 22(4):757–766
- Han J-Q, Feng R-S, Li Y (2013) Microfabrication technology for non-coplanar resonant beams and crab-leg supporting beams of dual-axis bulk micromachined resonant accelerometers. *J Zhejiang Univ Sci C Comp Electron* 14(1):65–74
- Heng L, Li MR (2013) Self-oscillation loop design and measurement for an MEMS resonant accelerometer. *Int J Adapt Control Signal Process* 27(10):859–872
- Li B, Zhao Y, Li C (2017) A differential resonant accelerometer with low cross-interference and temperature drift. *Sensors* 17(1):178
- Park U, Rhim J, Jeon JU (2014) A micromachined differential resonant accelerometer based on robust structural design. *Microelectron Eng* 129(11):5–11
- Park B, Lee SW, Han KJ (2016) Response characteristics of a MEMS resonant accelerometer to external acoustic excitation. In: 15th IEEE Sensors Conference, Orlando, FL, Oct 30–Nov 03
- Pedersen CBW, Seshia AA (2004) On the optimization of compliant force amplifier mechanisms for surface micromachined resonant accelerometers. *J Micromech Microeng* 14(10):1281–1293
- Seshia AA, Palaniapan M, Roessig TA (2002) A vacuum packaged surface micromachined resonant accelerometer. *J Microelectromech Syst* 11(6):784–793
- Shi R, Jia F-X, Qiu A-P (2013) Phase noise analysis of micromechanical silicon resonant accelerometer. *Sens Actuators A Phys* 197(8):15–24
- Suminto JT (1996) A wide frequency range, rugged silicon micro accelerometer with overrange stops. *MEMS, Sunnyvale*, pp 180–185
- Verma P, Khan KZ, Khonina SN (2016) Ultraviolet-LIGA-based fabrication and characterization of a nonresonant drive-mode vibratory gyro/accelerometer. *J Micro Nanolithogr Mem Mem* 15(3):035001
- Wang Y, Ding H, Le X (2017) A MEMS piezoelectric in-plane resonant accelerometer based on aluminum nitride with two-stage microleverage mechanism. *Sens Actuators A Phys* 254(2):126–133
- Yan B, Liu Y, Dong J (2016) The optimization of drive and sense circuit in silicon micro-machined resonant accelerometer. In: IEEE Chinese Guidance, Navigation and Control Conference (CGNCC), Nanjing, Peoples Republic of China, 12–14 Aug, pp. 2058–2063
- Yang B, Dai B, Zhao H (2014) A new silicon triaxial resonant microaccelerometer. In: International Conference on Information Science, Electronics and Electrical Engineering (ISEEE), Shandong Normal University, Sapporo, Japan, 26–28 Apr, pp. 1282–1285
- Zhang J, Su Y, Shi Q (2015) Microelectromechanical resonant accelerometer designed with a high sensitivity. *Sensors* 15(12):30293–30310

- Zhao L, Dai B, Yang B (2016) Design and simulations of a new biaxial silicon resonant micro-accelerometer. *Microsyst Technol Micro Nanosyst Inf Storage Process Syst* 22(12):2829–2834
- Zotov SA, Simon BR, Trusov AA (2015) High quality factor resonant MEMS accelerometer with continuous thermal compensation. *IEEE Sens J* 15(9):5045–5052
- Zou X, Seshia AA (2015) A high-resolution resonant mems accelerometer. In: 18th International Conference on Solid-State Sensors, Actuators and Microsystems (Transducers), Anchorage, AK, 21–25 Jun, pp. 1247–1250